NEUTRON SPECTRA, RECOIL MOMENTA AND
π° PRODUCTION CROSS SECTIONS FOR REACTIONS
INDUCED BY 10-100 MeV/NUCLEON HEAVY IONS

M. Blann
Lawrence Livermore National Laboratory
University of California
Livermore, CA   94550

Lawrence
Livermore
National
Laboratory

DISCLAIMER

NEUTRON SPECTRA, RECOIL MOMENTA AND Π° PRODUCTION CROSS SECTIONS FOR REACTIONS INDUCED BY 10-100 MeV/NUCLEON HEAVY IONS

M. Blann
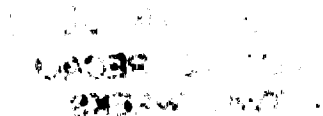Lawrence Livermore National Laboratory
University of California
Livermore, CA 94550

The Boltzmann master equation model has been applied to the question of precompound nucleon de-excitation of reactions induced by 10-100 MeV/nucleon (c.m.) heavy ions. Test systems of ^{16}O + ^{60}Ni and ^{27}Al + ^{86}Kr were selected. Experimental neutron spectra in coincidence with evaporation residue and fission fragments from the ^{20}Ne + ^{165}Ho system (due to Holub, et al.) were reproduced quite well by the master equation with exciton numbers between 20 and 23. Results show major fractions of the excitation and up to 35 nucleons removed during the coalescence-equilibration period. The linear momentum transfer predicted by the master equation is shown to be in good agreement with a broad range of data. Extension of the master equation to predict sub-threshold Π° production cross sections is shown to give satisfactory agreement with a large number of experimental results.

I.   INTRODUCTION

A very large experimental effort is being expended in the investigation of reactions induced by heavy ions of energies in excess of 10 MeV/nucleon. An important consideration in this energy range is the prompt nucleonic cascade which can greatly alter the excitation energy available for other processes, e.g. fission-like, or phenomena due to a somewhat relaxed composite

NEUTRON SPECTRA, RECOIL MOMENTA

M. Blann, Phys. Rev. C31, 1245 (1985), and M. Blann, UCRL–92802 (1985), unpublished.

2. MASTER EQUATION MODEL

2.1 Boltzmann Master Equation

The code which we use was written by Harp, et al.[1,2] to consider the relaxation to equilibrium of high energy nucleon induced reactions. It was later used by Harp and Miller[2] for investigating precompound decay for nucleon induced reactions in the region of a few tens of MeV of excitation. This code was modified by Harp and Blann for use in heavy ion reaction studies.[3,4]

The code used considers a two component (neutron and proton) fermion gas. An energy space is considered which is initially filled below the Fermi energy. Excitation energy is introduced into the system by bringing nucleons into the potential well in positions above the Fermi energy. The relaxation of these particles by either internal nucleon–nucleon (N–N) scattering, or by emission into the continuum, is followed versus time using coupled differential equations deriving their rates from phase space considerations.

The set of coupled differential equations used, as stated, was for a two component fermion gas. However it is more easily summarized in terms of a one component fermion gas:

$$\frac{d(n_i g_i)}{dt} = \sum_{j,k,l} \omega_{kl,ij}\ g_k n_k g_l n_l (1-n_j) g_i g_j$$

$$- \sum_{j,k,l} \omega_{ij,kl}\ g_i n_i g_j n_j (1-n_k)(1-n_l) g_k g_l$$

$$- n_i g_i \omega_{i,i'} g_{i'} + \frac{d}{dt}(n_i g_i^{fus}) \ , \tag{1}$$

system. In order to interpret many of the observable reaction properties it is helpful to have a model which is useful in predicting this precompound nucleonic cascade background.

In the present work we will explore the application of the Boltzmann master equation using the code of Harp, Miller and Berne,[1,2] as modified by Blann and Harp to consider heavy ion reactions.[3,4] We will predict precompound nucleon decay properties of the projectile–target pairs $^{16}O + {}^{60}Ni$ and $^{27}Al + {}^{86}Kr$, at projectile energies of 10–100 MeV/nucleon (c.m.). In Section 2 we will review the master equation model, and in particular the key question of the parameters which may influence the initial exciton energy distribution as the target–projectile pair makes contact and coalesces. In Section 3 we will present results of the calculations for the two sample systems selected. We will include estimates of the linear momentum transfer, which will be compared with experimental results for various projectile–target pairs. In Section 4 we will summarize our results, and discuss the types of experimental measurements which would test the model under consideration more rigorously as to its ability to reproduce the main aspects of the physics involved, and which might also permit improvements in the important exciton distribution assumption which contains much of the detailed mechanistic information of the model.

In Section 5, we describe the extension of the Boltzmann master equation to treating sub-threshold pion production, and the additional uncertainties of and sensitivity to parameter inputs due to the addition of this three body channel. Results of these calculations for a large number of heavy ion reactions are presented in Sec. 7, and conclusions on this approach for treating subthreshold pion production are given in Sec. 8. The text, figures and tables to be presented are based on, and largely taken from,

where n_i is the average occupation number and g_i the number of single particle states per MeV in an energy interval centered at i MeV above the bottom of the compound nucleus well. The $\omega_{ab,cd}$ are the transition probabilities for nucleons in initial states a and b to scatter into final states c and d; they are evaluated from free nucleon–nucleon scattering cross sections. The fractional occupation numbers $(g_i - n_i g_i)$ which multiply the free nucleon–nucleon collision rates give the Pauli exclusion correction. The $\omega_{i,i}'$, give the rate for a particle at energy i within the nucleus to go to energy i' outside the nucleus. The first two terms of Eq. (1) give the rates of scattering particles into and out of the interval i by two body (N–N) collisions, while the third term gives the rate of emission into the continuum. If this emission takes place before an internal equilibrium nucleon distribution is attained, the contribution is part of the precompound spectrum. (An equilibrium distribution is characterized by an equal a–priori population of every possible particle–hole configuration.) For details of quantitative input to the relevant transition rates we refer to earlier works.[1,2]

The fourth term in Eq. (1) contains a major portion of the physics in applying the master equation to heavy ion reactions. It represents the time dependent injection of excitons into the coalescing system. This should involve the microscopic aspects of the energy dissipation mechanism, and makes the model useful in testing energy dissipation models. In this work, as in earlier work, we will make simple phase space arguments similar to those used in exciton models over the past decade.[4−6] We discuss the evaluation of the 'injection' term of Eq. (1) in the next subsection.

2.2 Exciton Injection Distributions

The basis of our approach is the assumption that, for the interacting nuclei, the center of mass and Fermi momenta of the

participant nucleons may couple in an equal a-priori, energy conserving fashion.[6] This is an extension of the argument used in precompound decay models in which, e.g. an α projectile is characterized by a 4 exciton distribution. But we must consider the ways in which a heavy ion reaction differs from a light projectile induced reaction, so that we may judge success in our heavy ion reaction test with consideration of our uncertainty limits. We therefore next engage in a speculative discussion of this point.

In a nucleon induced reaction, we may clearly view the process as one exciton (the projectile) entering the nuclear potential. It may either be emitted, or it may scatter internally. This is clearly a one-exciton initial configuration which may go to the three, five etc. exciton configurations via two body interactions. Consider next a collision between symmetric heavy ions (e.g. Kr+Kr). Here as the nuclei come into contact, neither nucleus is clearly the target and the other the projectile. Nucleons will be expected to pass back and forth between both partners.[7] We might therefore expect a larger number of degrees of freedom (exciton number) to characterize this reaction relative to the 'projectile' nucleon number than for a nucleon or α induced reaction. In addition collective degrees of freedom may be important in the heavy ion reaction.

For nucleon induced reactions it is clear that the exciton phase space properly includes the capture Q value. For heavy ion reactions the di-nuclear shape is very deformed during the early stages of interaction during which nucleonic relaxation is expected to begin taking place.[8] This shape is far from the compound nucleus equilibrium shape, and therefore a significant amount of excitation may be unavailable for nucleonic (exciton) excitation. Additionally, large amounts of rotational energy may be unavailable to nucleon excitation in heavy ion reactions.[9]

These collective effects are expected to be dependent on the particular target–projectile combination, impact parameter and bombarding energy.

It is clear that the exciton distribution for heavy ion reactions is not expected to be as straight–forward as for light ion induced reactions. The real challenge may be in the formulation of reaction models for the dissipation process to give time dependent exciton spectra which may be used in Eq. (1) to generate nucleon emission spectra, which in turn may be compared with experimental results. The dynamics of the coalescence process may be important in determining the exciton spectra; however in this work we will simply use distributions characterized by exciton numbers which seem to give a reasonable reproduction of some experimental results, in order to generate extrapolated results. We will use single exciton numbers to represent the initial energy partitions, recognizing that careful considerations of the problem would lead at least to distributions represented by weighted sums over a range of exciton numbers, with some additional energy constraint for collective effects. We do this because our goal is use of the master equation to provide first order guidance of the expected nucleon cascade, rather than to solve the problem of microscopic injection. We feel that more extensive experimental results are necessary to guide the microscopic modelling.

The absolute maximum energy a single exciton could have as two heavy ions begin to coalescence would be the excitation energy of the compound nucleus, if it were formed; of course we would expect a vanishingly small probability of such a rare coupling. Energy tied up in collective modes (rotation, deformation) would be expected to decrease the hypothetical maximum exciton energy below the compound nucleus value. The exciton

state density expression[10] apportions a maximum excitation energy E among p particles and h holes with equal a–priori probability of energy per exciton (where n=p+h is the exciton number):

$$N(E) = (E)^{n-1} / p\,!\,h\,!\,(n-1)\,!\,,$$ (2)

where the energy E is expressed in units of the excitation energy E^*, $E=gE^*$ and g is the single particle state density in levels/MeV. We will assume a hole number of zero for estimating initial exciton populations for heavy ion reactions.

We may integrate Eq. (2) over energy intervals of width ΔU to calculate the number of excitons in an energy interval between U and $U+\Delta U$,

$$N(U)\Delta U = [\,(E-U)^{n-1} - (E-U-\Delta U)^{n-1}\,] / E^{n-1}\,.$$ (3)

Equation (3) was used in earlier works[4] for treating heavy ion reactions, where it was assumed that some number of projectile excitons n(t) entered the exciton mix at time t; n(t) multiplied by Eq. (3) gives the energy distribution of these excitons, and this be– came the injection term of Eq. (1). The number n(t) for neutrons (protons) was calculated as the projectile neutron (proton) number times the fractional volume of the projectile which would pass through a plane in a single time increment (which in our calcula– tions is $2x10^{-23}$ sec) at a constant velocity determined by the center of mass velocity at the top of the coulomb barrier. We would expect realistic coalescence dynamics to cause large excursions from this value (mainly to longer mix times); however increasing the coalescense period does not significantly affect the results of calculations with Eq. (1).

Use of Eq. (3) involves the implicit assumption that a single exciton may (with very minimal expectation) have the full energy

available. This is quite reasonable for a nucleon induced reaction for which the incident nucleon begins with the full energy. However for heavy ion reactions each nucleon has but a small fraction of the total energy. We argue that coupling with the Fermi motion makes a large portion of this energy available.[6] Consider as an example a reaction induced on a very heavy target by 10 MeV/nucleon ^{20}Ne. The total available excitation energy would be $\approx$200 MeV (if there were no collective restrictions). Yet if the Fermi energy were a maximum of 40 MeV, the maximum nucleon energy would be expected to be nearer $(\sqrt{10}+\sqrt{40})^2$ = 90 MeV. If nucleons in the half density nuclear region were primarily responsible for the precompound processes, a lower effective Fermi energy and lower maximum exciton energy might be appropriate. The density region over which nucleon exchange is taking place is a significant consideration for the ultimate use of model calculations of the type presented herein.

These considerations would suggest that Eq. (3) be replaced by a distribution function giving the number of excitons in a given energy range when there is an equal a–priori distribution of energy, but with the constraint that no exciton may have more than some energy F. If C(E,n,F) is defined as the number of ways of distributing E identical objects (energy quanta) among n cells (excitons) such that no cell has more than F objects,

$$P(U) = \frac{C(E-U,n-1,F)}{C(E,n,F)} \quad . \qquad (4)$$

The value of C(E,n,F) is given by:

$$C(E,n,F) = \frac{1}{E!} \frac{d^E}{dx^E}(1+x+x^2 \ldots x^F)^n \quad . \qquad (5)$$

8

We have used a subroutine[11] based on Eqs. (4) and (5) to provide the injection term of Eq. (1) in order to investigate the consequences of Fermi coupling constraints on the exciton distribution function. We find that this constraint versus Eq. (3) is not important, and have used Eq. (3) in this work except where otherwise noted.

3.   Exciton Injection Parameters

Before performing fairly global predictive calculations with the master equation model, we must consider how well experimental data are reproduced by this approach. Ideally we would like to test the model versus neutron and proton spectra in coincidence with evaporation residues, for incident heavy ions of energies in excess of 10 MeV/nucleon and over the entire energy range of interest. Some data are available for the reaction of ^{20}Ne + ^{165}Ho. In particular precompound neutron spectra in coincidence with fission fragments and evaporation residues were reported for 220, 290 and 402 MeV incident ^{20}Ne energy.[12]

In Fig. 1 we compare experimentally deduced spectra with results of the master equation calculation of Eq. (1) using Eqs. (4–5) for the exciton injection spectra, assuming that either 20 or 23 excitons partition the available excitation. The upper limits of excitation energy were used, i.e. the compound nucleus values which were 164, 228 and 326 MeV for incident ^{20}Ne energies of 220, 292 and 402 MeV, respectively. The experimental, angle integrated results shown in Fig. 1 are based on a Maxwellian fit to the high energy neutron spectra; the evaporation like component (which is partially included in our calculated result) is not included in the experimental spectra of Fig. 1. The calculated results of Fig. 1 are absolute and un-normalized. The phase space arguments previously stated, coupled with the unadjusted
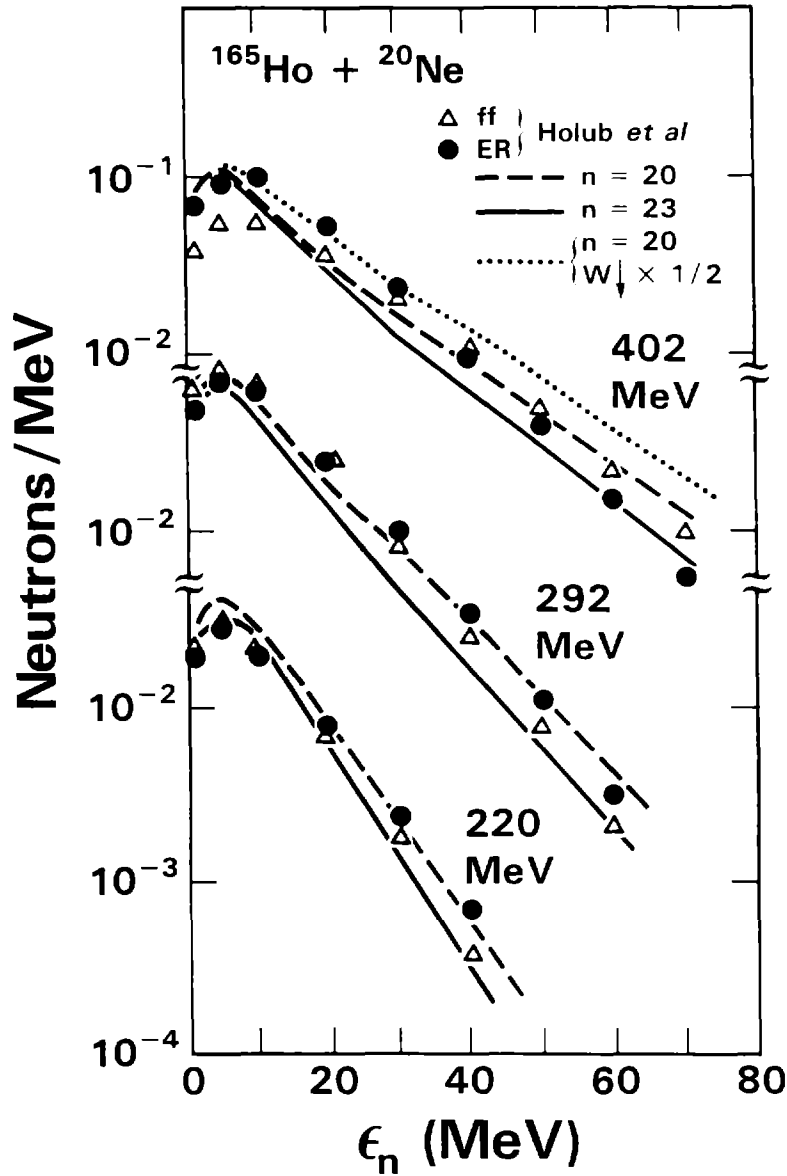
FIG. 1. Experimental and calculated precompound spectra for reactions induced by 220, 292 and 402 MeV(lab) ^{20}Ne ions on ^{165}Ho. The experimental points from Ref. (12) represent neutron spectra in coincidence with evaporation residues (open triangles) and fission fragments (closed circles). Calculated results are for initial exciton numbers of 20 (dashed curves) and 23 (line). A calculation using 20 excitons with the intranuclear transition rate divided by two is shown as a dotted curve for the 402 MeV case. All results are compared on an absolute, un-normalized basis.

nucleon–nucleon scattering cross sections which give the 'spreading' rate, yield the results of Fig. 1. The degree of agreement between calculated and experimental spectra is somewhat subjective. We feel that the 20 exciton result is satisfactory for all three bombarding energies. The experimental results certainly seem 'bracketed' by the 20 and 23 exciton results. (The trend of differences between experimental ER and fission coincident neutron spectra are suggestive of increased rotational energy with increased beam velocity for the fission–gated spectra.) Based on these observations we will use n_o = A_p and A_p + 3 for the calculations to be performed on the ^{16}O + ^{58}Ni and ^{27}Al + ^{86}Kr systems, giving a range of results, and indicating the sensitivity of results to the exciton number parameter.

For the case of 402 MeV incident ^{20}Ne energy we have performed a calculation (n_o = 20) in which the intranuclear transition rate was half the default value. This would approximate the result expected if the nucleon exchange took place predominately in nuclear matter of considerably less than half–density. This result (Fig. 1) may be seen to overestimate the experimental yields. Higher n_o values would be required to get better agreement at the higher neutron energies with the reduced intranuclear transition rate. This may be the reason that Holub et al. found higher 'best' exciton numbers than we find in this work, in their otherwise similar analyses of their spectra.[1,2]

Figure 1 indicates that the master equation gives a quite reasonable prediction of the high energy precompound nucleon spectra over a reasonably broad range of excitation. We will therefore use this approach to estimate some characteristics of the precompound cascade in heavy ion reactions both within this excitation range and beyond it. While it would be beneficial to have spectra similar to those of Fig. 1 to assess the validity of the

calculation at higher energies, we are not aware of the availability of such data. We therefore proceed, leaving open the question of microscopic modelling of dynamic collective effects and their influence on the exciton distributions.

3. RESULTS AND DISCUSSION

In the previous section it was shown that the master equation calculation gives a quite satisfactory reproduction of the precompound neutron spectra for the systems analyzed (Fig. 1), with the parameter for the initial exciton selected to be equal to or several units greater than the projectile mass number. We now proceed to use the master equation as a tool to give a gross guide to the question of energy and nucleon loss during the coalescence–equilibration process, using an exciton number parameter based on the analysis of the preceding section.

We will consider two systems differing somewhat in mass and charge, $^{16}O + {}^{60}Ni$ and $^{27}Al + {}^{86}Kr$. A range of energies from 10 MeV/nucleon to 100 MeV/nucleon (c.m.) will be considered in order to show how the relaxation process changes with the available excitation energy. We will assume effective exciton numbers of 16 and of 19 for the ^{16}O induced reactions, and of 27 and of 30 for the ^{27}Al induced reactions. In subsection A we present a broad, general discussion of the de–excitation process; in subsection B, we consider the implications of the predicted nucleonic cascade on the average linear momentum transfer to the excited equilibrated reaction residues.

3.1 Precompound De-Excitation

The decay characteristics predicted by the master equation are displayed graphically in Fig. 2 for the Al + Kr system for the assumption of 27 initial excitons; results for both test systems are
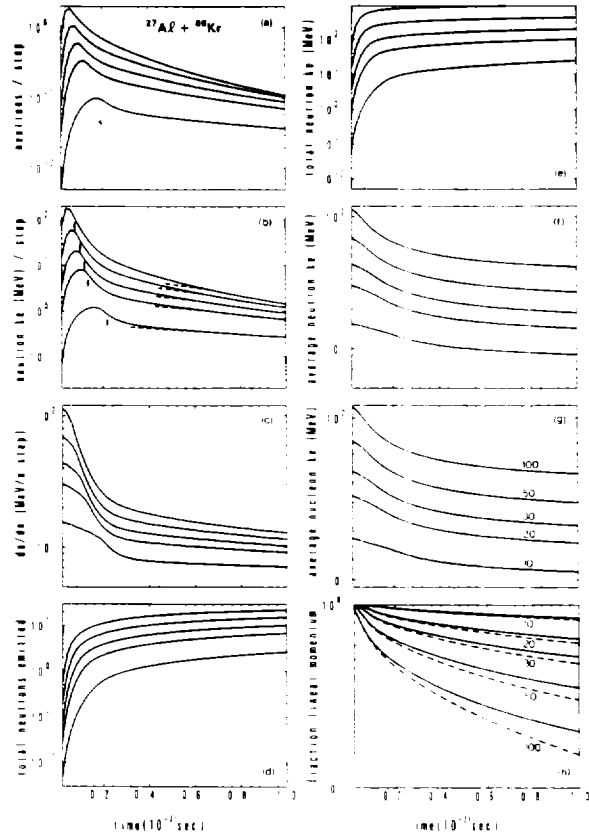
FIG. 2. Calculated precompound decay quantities versus time for reactions induced by 10, 20, 30, 50 and 100 MeV/nucleon (c.m.) ^{27}Al ions on ^{86}Kr. For each bombarding energy the figure shows the following versus time (a) the number of neutrons emitted during each time step (Δt) (2×10^{-23}sec) of the computation; (b) the kinetic energy removed by neutrons during each Δt; (c) the energy per neutron removed during each Δt (i.e. the quotient of (b) by (a)); (d) the total neutrons emitted up to time t; (e) the total kinetic energy removed by neutrons up to time t; (f) the average neutron energy of all neutrons emitted up to time t; (g) the average nucleon (neutron plus proton) kinetic energy removed up to time t; and (h) the fraction linear momentum remaining on the heavy residues up to time t. In (b) the up arrows indicate the time at which fusion was complete for each incident energy; the intersections of the dashed lines with the calculated curves were used to estimate an equilibration time. The incident energies are shown in (g) and (h). The ordering shown in (g) is valid for (a–g). In (h) the dashed curves represent the calculated linear momentum if it is assumed that all nucleons are emitted at 0° to the beam, i.e. if the angular correction of Eq. (6) is not made.

13

summarized in Tables I – II for $n = A_p + 3$, and in Tables III – IV for $n = A_p$. The graphs in Fig. 2 show many of the predicted decay properties vs. time for the example shown; characteristics of proton emission are similar to neutron emission. Similarly the $^{16}O + {}^{60}Ni$ system has the same features as the Al + Kr system. For these reasons we exhibit only one figure of this type. Discussion of Fig. (2h), linear momentum transfer, and of additional assumptions necessary to its calculation, is deferred to the following subsection. Results similar to those shown in Fig. 2 for proton emission are available from the calculation and are summarized in Tables I – IV.

The time at which the infusion of nucleons from the projectile to the composite system is complete is indicated in Fig. 2b and in Tables I – IV. Determining the approximate time at which a given system has equilibrated is more subjective. We have taken the results in Fig. 2b and extrapolated the linear regions of the curves at long times to shorter times. The region first showing an acceleration in the rate of neutron emission is taken as the equilibration time. Dashed curves have been added in Fig. 2b to illustrate this procedure. The times for fusion and for equilibration are summarized in Tables I – IV. Both start from time zero defined as the time of the initial target–projectile contact, i.e. the beginning of the coalescence process.

In Tables I – IV we have multiplied the neutron (proton) multiplicities for precompound nucleons by the neutron (proton) binding energies. With the implicit assumption that the values used in the calculations represent reasonable averages, this allows us to estimate the total (kinetic plus binding) energy removed during equilibration. These results are summarized graphically in Fig. 3. One interesting trend in Fig. 3 is the decrease in rate of precompound excitation removal above 50 MeV/nucleon. For the

NEUTRON SPECTRA, RECOIL MOMENTA

TABLE I. Calculated decay prior to equilibration for reactions of $^{27}Al + {}^{86}Kr$ assuming a 30 exciton partition

E_{lab} (MeV)	^{27}Al t_{eq} $\cdot 10^{22}$ (sec)	t_{fus} $\cdot 10^{22}$ (sec)	$\dfrac{p11^a}{P_{beam}}$	Δl^b ($\hbar$)	N_n^c	N_p^d
355	4.7	2.2	0.92	13	1.28	0.65
710	4.8	1.4	0.79	48	3.95	2.42
1065	5.1	1.2	0.67	92	6.74	4.41
1775	6.6	1.0	0.48	187	12.2	8.47
3350	7.8	0.8	0.28	355	20.0	14.5

KE_n^e (MeV)	KE_p^f (MeV)	ΔE^g (MeV)	$\Delta E/E^h$	v_{rel}^i	$(E/A)_{c.m.}$ (MeV/nucleon)
12.2	10.4	40	0.15	3.1	10
62	54	170	0.32	4.8	20
137	121	350	0.44	6.0	30
334	295	800	0.60	7.9	50
826	720	1830	0.68	10.8	100

[a] estimated fraction of linear momentum transfer
[b] angular momentum removal prior to t_{eq}
[c] number of neutrons emitted prior to t_{eq}
[d] number of protons emitted prior to t_{eq}
[e] neutron kinetic energy removed prior to t_{eq}
[f] proton kinetic energy removed prior to t_{eq}
[g] sum of neutron plus proton kinetic and binding energy removed prior to t_{eq}
[h] ratio of energy removed by precompound particle emission to total available compound nucleus excitation energy
[i] $\surd$ $(E_{LAB}-V)/A_p$ where V is the coulomb barrier and A_p the projectile mass number (27)

15

TABLE II. Calculated decay prior to equilibration for reactions of ^{16}O + ^{60}Ni assuming a 19 exciton energy partition (column headings are as defined in Table I.

E_{lab} ^{16}O (MeV)	t_{eq}•10^{22} (sec)	t_{fus} •10^{22} (sec)	$\frac{p11}{P_{beam}}$	Δl (ℏ)	N_n	N_p
141	3.8	2.2	0.98	1	0.16	0.20
218	3.8	1.8	0.94	5	0.52	0.56
314	4.2	1.4	0.88	12	1.05	1.15
800	5.0	0.8	0.64	59	4.05	4.15
1013	6.0	0.8	0.54	85	5.5	5.6
1600	6.1	0.6	0.41	137	8.0	8.0
2027	6.2	0.6	0.36	167	9.2	9.1

KE_n (MeV)	KE_p (MeV)	ΔE (MeV)	$\Delta E/E$	v_{rel}	$(E/A)_{c.m.}$ (MeV/nucleon)
1.15	2.4	6.6	0.06	2.4	7.0
5.2	8.3	23	0.13	3.2	10.8
13.7	20.4	54	0.22	4.1	15.5
99	119	291	0.46	6.9	39.5
153	179	431	0.54	7.8	50.0
305	332	780	0.62	9.8	79.0
408	435	1007	0.63	11.1	100.0

TABLE III. Calculated decay prior to equilibration for reactions of ^{27}Al + ^{86}Kr for n = 27 (column headings are as defined in Table I.

E_{lab} (MeV)	^{27}Al $t_{eq} \cdot 10^{22}$ (sec)	$t_{fus} \cdot 10^{22}$ (sec)	$\dfrac{p11}{p_{beam}}$	Δl (ħ)	N_n	N_p
355	4.8	2.2	0.91	15	1.54	0.81
710	5.4	1.4	0.74	59	4.85	3.02
1065	5.6	1.2	0.62	106	7.8	5.2
1775	6.6	1.0	0.42	209	13.3	9.26
3350	6.8	0.8	0.26	365	20.0	14.6

KE_n (MeV)	KE_p (MeV)	ΔE (MeV)	$\Delta E/E$	v_{rel}	$(E/A)_{c.m.}$ (MeV/nucleon)
15.7	13.5	49	0.19	3.1	10
79	70	215	0.41	4.8	20
167	148	424	0.53	6.0	30
389	343	919	0.69	7.9	50
898	780	1964	0.73	10.8	100

TABLE IV. Calculated decay prior to equilibration for reactions of ^{16}O + ^{60}Ni for n = 16 (column headings are as defined in Table I.

E_{lab} ^{16}O (MeV)	$t_{eq} \cdot 10^{22}$ (sec)	$t_{fus} \cdot 10^{22}$ (sec)	$\frac{p11}{p_{beam}}$	Δl (ℏ)	N_n	N_p
202	5.0	1.8	0.92	7	.61	0.69
405	5.0	1.4	0.76	24	2.21	2.35
606	5.6	0.8	0.62	62	3.84	3.96
1013	6.0	0.8	0.45	102	6.4	6.44
2027	6.4	0.6	0.27	190	10.1	9.9

KE_n (MeV)	KE_p (MeV)	ΔE (MeV)	$\Delta E/E$	v_{rel}	$(E/A)_{c.m.}$ (MeV/nucleon)
6.5	10.7	28.6	0.18	3.1	10
38	51	129	0.40	4.1	20
85	105	259	0.54	6.9	30
201	227	543	0.68	7.8	50
489	514	1182	0.74	11.1	100

case $n_o = A_p$, the fractional results shown in Fig. 3 are not distinguishable for the two systems under consideration.

The Figures and Tables show a rapid increase of precompound decay as projectile energies exceed 10 MeV/nucleon, as was pointed out earlier.[3,4,6] The systems may be seen to
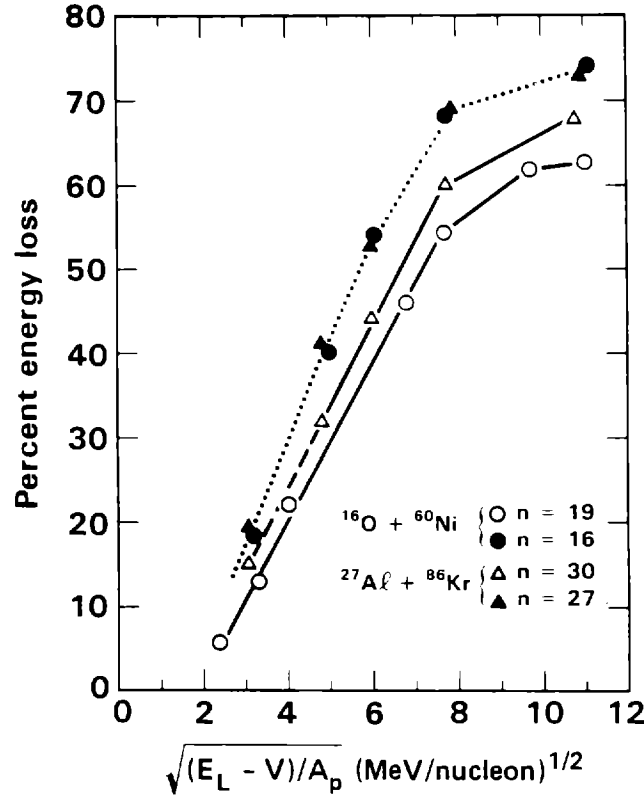
NEUTRON SPECTRA, RECOIL MOMENTA

FIG. 3. Percent energy loss versus relative velocity for ^{16}O + ^{60}Ni and ^{27}Al + ^{86}Kr at c.m. energies of 10–100 MeV/nucleon. Calculated points from Tables I – IV are shown versus the relative velocity (abscissa) as defined in Table I. The calculated points have been joined by straight line segments as a visual guide. Calculated results are for initial exciton numbers equal to the projectile mass number (dotted curve) or three greater than the projectile mass number (solid and dashed curves).

relax rapidly toward equilibrum following the conclusion of coalescence, i.e. in periods of the order of 2–$5 \cdot 10^{-22}$ sec. Nonetheless these periods are in the range of the collective times required to go from contact to an equilibrium composite configuration (particularly in the 'extra' push region), and from the compound shape to saddle. Many nucleons may be emitted

19

during this time, considerably altering both the excitation energy and angular momentum of the hot, equilibrated residues. For example, for Al + Kr at 100 MeV/nucleon, our model calculation predicts approximately 35 nucleons (and probably additional d, t, α etc. clusters) removed during this short period, and 1800 of the 2700 MeV of maximum available excitation removed. Interpretation of e.g. coincident fission fragments in such an experiment would therefore suggest an analysis in terms of a much cooler fissioning system, and of significantly lower mass, than given by the composite system mass and c.m. projectile energy. Precompound decay of nucleons should become of major importance as projectile energies go beyond 30 MeV/nucleon, and it is predicted to be a very significant process at somewhat lower energies.

3.2 Fractional Linear Momentum Transfer and Angular Momentum Decrement

3.2.1. Linear momentum transfer. The precompound nucleonic cascade described thus far should be related to the momentum transfer in heavy ion reactions. The factors necessary to completing the relationship which have not yet been addressed are the angular distribution of ejectiles and the contributions of non-nucleon ejectiles, e.g. α, d, t etc. (A preliminary discussion of the linear momentum transfer question has already appeared.)

We will make some very simple assumptions and approximations for these points. For the angular distribution of nucleons, we begin by considering a diffraction limit to the angular distribution as first suggested by Mantzouranis et al.,[13]

$$R\Delta\theta \geq \hbar/k \tag{6}$$

where R is the nuclear radius, $\Delta\Theta$ the angular uncertainty, and k the nucleon wave number. In Fig. 12 of Ref. (14), we show the half angle $\Delta\Theta$ of Eq. (6) as a function of nucleon energy and nuclear mass number. In Figs. 16 and 17, from the previous article and also from Ref. (14), we show the experimental angular distributions for neutrons of 9 and 14 MeV from the ^{90}Zr (p,n) reactions with 25 MeV[15,16] incident protons, and for 20 and 30 MeV neutrons with 45 MeV incident protons.[16] The dotted curves in Figs. 16 and 17 represent the results of a calculation for which it was assumed that nucleons entering or leaving the nucleus are uniformly scattered (due to quantal processes) over a half angle $\Delta\Theta_{1/2}$ given by Eq. (6). For the case of a nucleon entering followed by a nucleon leaving the nucleus, we have folded the single scattering kernel with itself under the assumption that quantal phenomena such as refraction will be present in both entrance and exit channels. Greater detail and discussion of these results are to be found in Ref. 14. It may be seen that this result gives a quite good representation of the angular distributions over an angular range containing $\approx 80\%$ of the cross section.

The calculation used in generating the angular distributions in Figs. 16 and 17 is too computationally tedious to use in the master equation approach, but does demonstrate that the diffraction angle limit is a reasonable one. Therefore we calculated the momentum decrement due to nucleon emission by multiplying the nucleon momentum by $\cos(\Delta\Theta)$ from Eq. (6),

$$P_{11} = \sqrt{2M\epsilon} \cdot \cos(\Delta\Theta) \tag{7}$$

if $\Delta\Theta \leq 90°$, and by zero if $\Delta\Theta > 90°$. A value of $\Delta\Theta > 90°$ still will represent some forward peaking of the angular distribution. However the forward peaking becomes slight when this is the

case, so we make the isotropic assumption stated above for nucleons with a broad angular distribution. Figure 12 of the previous article shows that these will be nucleons of a few MeV which should have undergone considerable relaxation toward equilibrium. In Eq. (7), M represents the nucleon mass and ε the kinetic energy.

The second point to consider is the influence of the emission of clusters such as d, t, α etc. on the emission cascade. We have made a minimum correction to the momentum loss from the nucleon–cascade based on cluster multiplicities measured for reactions induced by 39, 62 and 90 MeV protons on a wide range of targets.[17,18] The ratios p:d:t:^{3}He:α was found roughly to be 10:1:0.02:0.02:0.5. We have used this ratio, assumed that it holds equally well for the neutron as well as proton cascade, and assumed a cluster kinetic energy of half the nucleon kinetic energy. This increases the momentum decrement by 8% over the pure nucleon cascade result. Because the correction under discussion is a small fraction of the total, a fairly large uncertainty in the assumed intensities and average energies would not seriously alter the results. Two points should be mentioned in this regard. The first is that in the inclusive measurements of Awes et al.[19] for ^{16}O + ^{197}Au, cluster multiplicities very much larger than those assumed in this work were observed. The second point is based on the model prediction of Bisplinghoff et al.[20] that high angular momenta should significantly enhance precompound cluster emission. In view of these considerations we must view our results as lower limits to the linear momentum loss, and observe that spectra of nucleons and clusters in coincidence with evaporation residues and fission fragments would be very valuable in constraining results of model precompound decay calculations of linear momentum transfer in heavy ion reactions.

NEUTRON SPECTRA, RECOIL MOMENTA

Results of the linear momentum calculation described are shown in Fig. 4 for the two test systems selected in this work. Various experimental results[21-31] are also shown in Fig. 4. Reference to Fig. 2g shows that the momentum transfer value has some sensitivity to the time assumed for equilibration. There is therefore some uncertainty in the calculated value due to subjectivity in selecting an equilibration time, and indeed all results quoted probably have a ± 10% uncertainty for this reason alone. Nonetheless, the calculated results based on the simple phase space master equation model of Eqs. (1-2) are in very good agreement with the experimental results. We hope that this, coupled with the generally satisfactory reproduction of precompound nucleon spectra using exciton numbers in a reasonable range, suggests that the model reproduces the main aspects of the precompound-relaxation physics, although surely not the finer details! If this is so we might also estimate rough values of the angular momentum removed by the precompound cascade, as this could considerably alter the macroscopic trajectories of the interacting target-projectile systems. We consider this question in the following subsection.

3.2.2. Angular momentum decrement in precompound cascade. In the previous subsection we presented results based on the estimated forward component of momentum removed by the precompound decay cascade. This is semiclassically related to the angular momentum decrement by

$$l(\hbar) = p \cdot R = p_{11} \cdot R \ . \tag{8}$$

Where p is the momentum decrement and p_{11} the decrement parallel to the beam. To get some rough estimates of the angular momentum decrement we need only select a value of the radius. This could be done in any number of ways, but let us simply
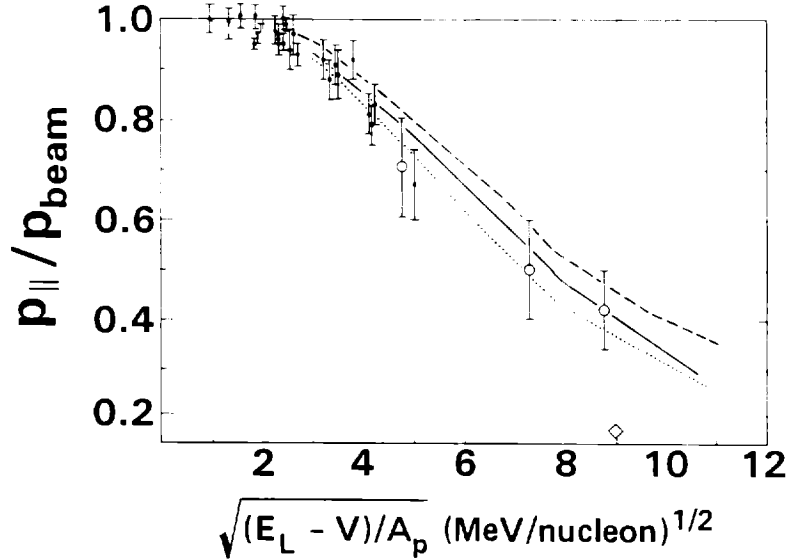
FIG. 4. Calculated and experimental linear momentum transfer
for heavy ion reactions at energies up to 100 MeV/nucleon (c.m.).
The ordinate gives the fraction linear momentum transfer; the
abscissa is relative beam velocity as defined in Table I. The
experimental results shown by closed circles with error bars are
from the summary of Ref. (19); the original sources are to be
found in Refs. (20–27). The open points with error bars are from
Ref. (28), and the open triangle is from Ref. (29). The dashed
curve is the calculated linear momentum transfer for ^{27}Al +
^{86}Kr assuming a 30 exciton energy partition; the solid curve is
for ^{16}O + ^{60}Ni assuming a 19 exciton energy partition. The
dotted curve is for ^{27}Al + ^{86}Kr assuming a 27 exciton partition,
and for ^{16}O + ^{60}Ni assuming a 16 exciton partition.

assume the composite system mass and a spherical system (recog-
nizing that at very high angular momenta, equilibrium ground
state shapes may have semi–major axes in excess of twice the

spherical nucleus value). We will use an R_0 value of 1.5 x 10^{-13} cm, a 'square well' value. Then if we let f be the calculated fractional linear momentum transfer from Tables I – IV, based on Eq. (7), ϵ_p the laboratory projectile energy and A_p the projectile mass, the angular momentum removed by the precompound emission cascade may be estimated by

$$\Delta l(\hbar) \simeq [\, (1-f) \, \sqrt{2A_p \epsilon_p} \,] \, R$$

$$\simeq 0.34 \, (1-f) \, \sqrt{A_p \epsilon_p} \, A_c^{1/3} \, . \tag{9}$$

This is intended to give only a very rough estimate of the angular momentum removal possible due to the nucleon precompound decay. Results of using Eq. (9) for the two test systems are summarized in column 5 of Tables I – IV. It may be seen that very significant angular momentum decrements may result from the precompound decay; many higher partial waves in the entrance channel may lead to compound nucleus formation than might have been expected by ignoring this phenomenon. Similarly higher partial waves and rotational energies will affect the initial exciton–energy partition in the coalescence process. We should not, therefore, be discouraged by the fact that a single initial exciton number does not reproduce the precompound spectra at all bombarding energies. We must first understand the dynamics of the reactions better before drawing quantitative conclusions about the model. Perhaps some better understanding of the ranges of the exciton parameter value versus bombarding energy would result from an iteration over distributions calculated using excitation energies decreased by rotational energies, using Eq. (9) with the output to get a range of relevant partial waves.

4. CONCLUSIONS: BME FOR NEUTRON EMISSION AND MOMENTUM TRANSFER

We have used the Boltzmann master equation as a guide to the precompound nucleon emission cascade for reactions induced by heavy ions in the 10 to 100 MeV per nucleon region. The results will have a sensitivity to the initial exciton distribution assumed. As discussed, we do not understand all the macroscopic/microscopic details which would affect the exciton distribution, and the purpose of this work was not to investigate this potentially physically fertile area. Rather we wished to see how the energy and precompound nucleon emission might vary with projectile energy. Because our simple exciton distribution function is reasonably successful in reproducing the experimental precompound spectra, our calculations should give guidance as to the expected precompound decay cascade versus projectile energy.

The results of the calculations are summarized in the figures and in Tables I – IV. We see that very large fractions of the total energy are expected to be removed prior to equilibration at the higher energies considered, and that the residual composite system may have much lower angular momentum than is introduced in the entrance channel. This simple phase space calculation seems to give linear momentum transfer results which are quite consistent with experimental results.

Open questions include those of the multiplicities and spectral distributions of clusters emitted in coincidence with evaporation residue and fission fragments, and of the nucleon emission spectra for the same coincidence measurements. These data, extending beyond the 20 MeV/nucleon limit of Fig. 1, would allow better estimates of the reliability of the various calculated quantities summarized in Tables I – IV, and help decide if the

result of Fig. 4 should be viewed as an upper limit only, or as a proper estimate of the fraction linear momentum transfer. In this way the crude calculation presented should become a more reliable tool for predicting the precompound decay contribution to energetic heavy ion reactions, and in developing a convenient time dependent model.

5. PION PRODUCTION VIA NUCLEON–NUCLEON COLLISIONS IN THE BOLTZMANN MASTER EQUATION

A great deal of work has been done regarding experimental measurement and theoretical interpretation of 'subthreshold' pion production.[32-43] This involves reactions of heavy ions with beam velocities below the energy per nucleon required to produce pions in free nucleon–nucleon collisions, yet with the collective energy of the projectile bringing energy in excess of the pion mass to the composite system. The question is how the collective energy shared by many of the projectile nucleons becomes available for pion production.

One suggestion is that the coupling of the projectile beam velocity with the Fermi momenta of the nucleons gives enough energy to a few nucleons that they may undergo intranuclear collisions with sufficient energy to produce pions.[44] In the present work we will investigate the question as to whether or not such a mechanism is semi–quantitatively in agreement with existing experimental data. This will give an answer to the question 'might such a mechanism be responsible for the experimental results given reasonable input to the calculations?' It can not, of course, prove that this is the correct mechanism. We will investigate the question by following the relaxation process of the composite system via the Boltzmann master equation model (BME) originally encoded by Harp, Miller and

Berne.[1,2] We will also investigate the energy which this model predicts is removed during the equilibration process, as this is germane to model interpretations involving pion production from a compound nucleus (fully equilibrated) system.[35,36]

In Section 6 the changes to the master equation from the discussion of Section 2 and input sensitivity for pion production will be defined and discussed. In Section 7 we compare results of this equation with experimental measurements of π° produced from 35 MeV/nucleon ^{14}N on several targets, and from [12]C + [12]C, [58]Ni and [238]U reactions at energies of 60 to 84 MeV/nucleon and [40]Ar + [40]Ca, [119]Sn and [238]U at 44 MeV/nucleon. We will illustrate the dependence of results on input parameters, and suggest those experimental measurements which would help in reducing the uncertainties in the range of input variables. Conclusions will be presented in Section 8.

6.   BOLTZMANN MASTER EQUATION AND INPUT FOR PION PRODUCTION CALCULATION

The HMB code presented in Section 2 has been modified to include a channel in which three body final states may exist;[43] in particular

$$n + n \rightarrow n + n + \pi^\circ \qquad (10a)$$

$$p + p \rightarrow p + p + \pi^\circ \qquad (10b)$$

$$p + n \rightarrow p + n + \pi^\circ \qquad (10c)$$

$$p + n \rightarrow d + \pi^\circ \ . \qquad (10d)$$

The energy dependent cross sections (10b–d) which we use are from the work of Ver West and Arndt;[45] we assume that (10a) and (10b) have identical cross sections. We add the cross

sections (10c) and (10d) for π° production rates in p–n collisions. We calculate rates for these pion producing reactions by

$$\omega^{PP\pi^\circ}_{ij\to k'l'm} = \frac{\sigma_{PP\pi}d(\epsilon_i + \epsilon_j)\,[(2/M)\,(\epsilon_i^P + \epsilon_j^P)]^{1/2}}{V\sum_{nop}' g_n g_o g_p W(\epsilon_i^P + \epsilon_j^P - \epsilon_n^P - \epsilon_o^P - \epsilon_p^\pi - m_{\pi^\circ})} \tag{11}$$

with symbols defined in Table V, and with an analogous expression using $\sigma^{PN\pi^\circ}$ for neutron–proton collision processes.

The master equation (1) is then modified by a pion production term

$$\frac{dN^\pi}{dt} + \sum_{ijk'l'm} \omega^{PN\pi^\circ}_{ij\to k'l'm}\; g_m g_i^P g_j^P n_i^P n_j^P (1 - n_{k'}^P)(1 - n_{l'}^P)$$

$$+ \sum_{ijk'l'm} \omega^{PN\pi^\circ}_{ij}\; g_m g_i^P g_j^N n_i^P n_j^N (1 - n_{k'}^P)(1 - n_{l'}^N)$$

$$+ \sum_{ijk'l'm} \omega^{NN\pi^\circ}_{ij}\; g_m g_i^N g_j^N n_i^N n_j^N (1 - n_{k'}^N)(1 - n_{l'}^N) \quad , \tag{12}$$

with symbols defined in Table V. The sums are over all energy pairs i+j such that $k'+l'+m+m_\pi=i+j$. Implicit in this approach is the assumption that we may reasonably treat the final state as three body in nature near threshold, rather than as being dominated by a Δ final state. If this is not a good assumption, we feel that the shape of the final π° spectrum would be affected more adversely than the total production rate which depends primarily on the $\sigma^{PP\pi^\circ}$, $\sigma^{PN\pi^\circ}$, and $\sigma^{NN\pi^\circ}$ values versus incident nucleon energies. The threshold energy, i+j, for pion production is 280 MeV in our calculation.

TABLE V. Definition of symbols.

Symbol	Definition
$n_i^X \omega_i^X \to i$	fraction of population of the nucleons of type X (neutron = N, proton = P) emitted per unit time from a bin at energy i measured from the bottom of the Fermi sea.
$\omega_{ij \to k,l}^{XY}$	rate at which one nucleon of type X at energy i scatters with one nucleon of type Y at energy j into final energies k and l.
g_i^X	number of states for a particle of type X in a 1 MeV wide energy bin centered at energy i with respect to the Fermi energy.
n_i^X	fraction of the g_i^X levels in bin i which are occupied at time t.
B_X	binding energy of a nucleon of type X.
ϵ_i^X	single particle energy of a nucleon of type X in bin i, measured from the bottom of the Fermi sea.
$\omega_{i \to i'}^X$	rate at which a particle of type X at energy i with respect to the bottom of the nucleon well and energy i' with respect to the unbound continuum is emitted into the continuum.
$\omega(\epsilon_i^Y + \epsilon_j^P - \epsilon_k^P - \epsilon_k^P)$	unity when initial and final nucleon energies conserve energy, otherwise zero.
E^*	composite system excitation energy.
V	the nuclear volume, calculated in this work using a square well with radius parameter 1.2×10^{-13} fm.
M	nucleon mass.
$\sigma^{XY}(\epsilon_i + \epsilon_j)$	cross section for a free nucleon of type X and energy ϵ_i to collide elastically with a free nucleon of type Y and energy ϵ_j.
$\sigma^{XY\pi^o}(\epsilon_i + \epsilon_j)$	cross section for a free nucleon of type X at energy ϵ_i to collide with a nucleon of type Y at energy ϵ_j to produce a π^o plus nucleons X and Y with final energies such that mass and energy are conserved.

NEUTRON SPECTRA, RECOIL MOMENTA

The HMB model code was modified to use a time dependent injection of nucleons into a nuclear system, as might be encountered in a heavy ion reaction where nucleons from a projectile interact with target nucleons after passing through a neck region.[46,47] For simplicity we assume a projectile approach at constant velocity given by the projectile energy decreased by the coulomb barrier height. Results are not sensitive to the details of the assumed time dependence of the coalescence process, but they are very sensitive to the assumed energy dependence of the coalescing nucleon excitations.

For the latter we have made several assumptions. Results of calculations for pion production rates will be considerably more sensitive to the quantitative merit of these assumptions than will nucleon emission spectra. We will try to illustrate this point in the results to be presented. This exercise will point out the types of experimental measurements which might better restrict the range of input parameters for the pion production calculation.

Our assumptions for the initial exciton distribution function involve the following: the projectile nucleons have a beam velocity with which they approach the target. Additionally there is a velocity distribution of nucleons within the projectile due to the Fermi momenta. We assume that the projectile nucleons entering the target may therefore have energies from the target Fermi energy, to the target Fermi energy plus the maximum energy resulting from the coupling of the projectile Fermi and beam velocities, or the maximum excitation energy available to the composite nucleus, whichever is less. The distribution function used is based on the assumption that some number of excitons share the total available excitation energy with every allowed energy partition equally likely. The distribution function is discussed in greater detail in Section 2.

The agreement of calculated neutron spectra in Fig. 1 supports the assumed exciton distribution function as being in agreement with nature up to 70 MeV neutron energy, and probably somewhat beyond. However pion production requires collision of nucleons with 140 MeV or more above the bottom of the Fermi sea. We do not have evidence such as that of Fig. 1 to support our distribution function for the very tail of the exciton distribution function which is relevant to pion production. Measurements of the type shown in Fig. 1 to much higher neutron energies would provide the information necessary to an independently supported exciton distribution function to be used for pion production calculations. Such measurements are difficult because coincidence measurements are required, with the very small cross sections becoming ever smaller with increasing neutron energy. The evaporation residue like fragment would require detection with a large solid angle device (e.g. a recoil spectrometer) for such a coincidence measurement

The sensitivity of results of these calculations may be illustrated by comparing the distribution function versus energy for three cases. This is done in Fig. 5, where we show the distribution function for a ^{14}N projectile at 35 MeV/nucleon assuming 35 MeV projectile Fermi energy with 14 excitons, 40 MeV projectile Fermi energy with 14 excitons, and 35 MeV Fermi energy with 17 excitons. The pion production rate (14 excitons) increases by 60% between the distribution functions assuming 35 and 40 MeV projectile Fermi energy, due entirely to the small tail extending to higher energies in the latter case. The neutron spectra up to 70 MeV, on the contrary, are identical for either distribution function! Similarly in going from 14 to 17 excitons, the neutron spectra at 70 MeV will decrease by 40%, while the pion production rate will decrease by 70%. We see that there is a reasonably large uncertainty in results from
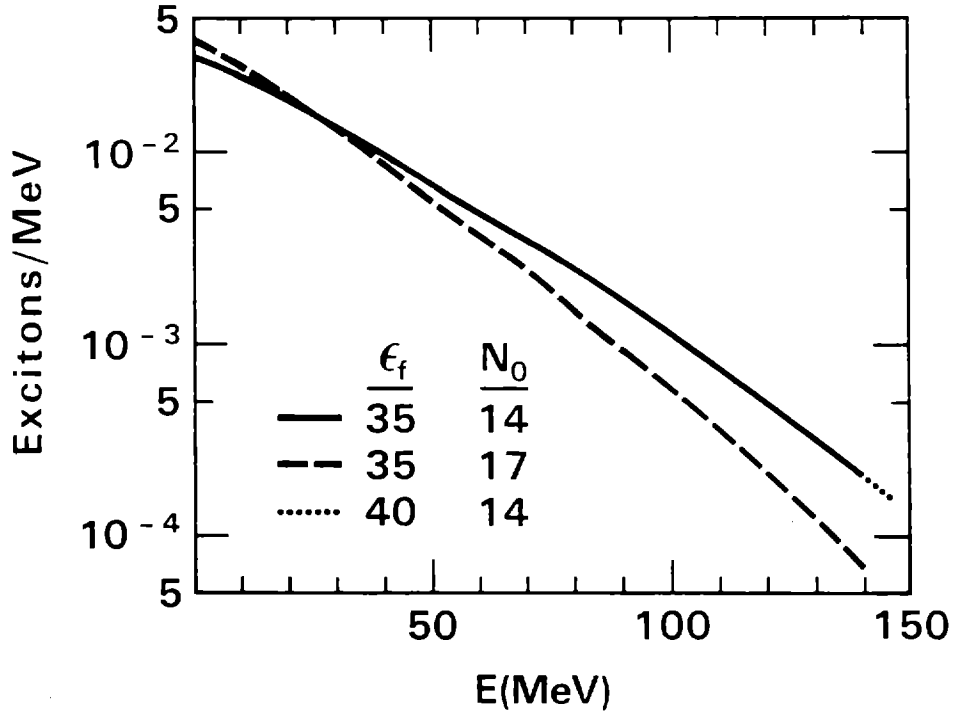
FIG. 5. Exciton density distribution versus energy for projectile Fermi energies (ϵ_f) of 35 and 40 MeV, assuming initial exciton numbers of 14 and 17.

calculations of the type we perform due to uncertainties in the input. Independent experiments (high energy nucleon emission spectra) may ultimately allow us to narrow the range of 'acceptable' input. At present we proceed to use what seem to be reasonable values, bearing in mind the uncertainties in final results arising due to our ignorance in the input. For results to be

presented (e.g. Table VI) we assume a target radius parameter of R_o = 1.2 fm (Fermi energy $\approx$30 MeV), and projectile Fermi energy of 35 MeV.

There is an additional point which must be emphasized as a possible weak point in the pion production calculation. The N–N collision cross sections are for average 90° collision angles; the Boltzmann equation as we use it follows energies, and not momenta. For pion production the high momentum components are most important, and these are more likely (initially) to be parallel rather than at 90°, when both partners are from the primal projectile source.

The calculation as described thus far provides a prediction of the number of pions produced per target–projectile interaction. Experimental measurements report the cross sections of emitted pions. These two points are connected by a bridge of additional assumptions. These primarily include the pion mean free path in nuclear matter, and the cross section for collisions which are sufficiently central to participate in the pion production process. Our approach to these questions is arbitrary and simple; the uncertainties already discussed do not justify very sophisticated answers.

The mean free path of a pion is thought to be reasonably independent of energy for pions above 20 MeV, with a mean free path of around 3 fm.[48] The average impact parameter for a reaction comes at around 0.7 of the maximum radius. We therefore have assumed pions produced at 0.7 x 1.2 x 10^{-13} (A_T + $A_p)^{1/3}$ cm. We assume that half the pions move radially away from the nuclear center and half toward the center. We calculate an energy attenuation factor, assuming a 3 fm mean free path, based on this simple picture. The values so calculated are summarized in Table VI. For the reaction cross sections we have used

TABLE VI. Summary of calculated and experimental subthreshold pion production cross sections.

MeV/Nucleon	σ_R (a)	f_{atten} (b)	Calculated Pions/Interaction	Emitted Pions (μb)(c)	EXPTL (b)	Ref	E* (MeV)g	$\bar{n}$(h)	n_0(i)
Projectile Target: $^{12}C/^{12}C$									
60	0.96	0.42	0.41×10^{-5}	1.4	1.7(3)	d	374	31	12
74			0.34×10^{-4}	14.0	8.5(10)	d	458	34	12
84			0.10×10^{-3}	40.0	19.(23)	d	518	36	12
Projectile Target: $^{12}C/^{58}Ni$									
60	1.72	0.34	1.9×10^{-5}	11.0	7.(1)	d	597	67	12
74		0.34	1.26×10^{-4}	74.0	31.(4)	d	736	74	12
84		0.34	3.0×10^{-4}	175.0	72.(9)	d	835	79	12
Projectile Target: $^{12}C/^{238}U$									
60	1.36	0.24	1.17×10^{-5}	9.2	13.(2)	d	661	133	12
74		0.24	5.9×10^{-5}	46.0	64.(10)	d	821	148	12
84		0.24	1.4×10^{-4}	110.0	174.(21)	d	936	158	12
Projectile Target: $^{14}N/^{27}Al$									
35	1.32	0.38	0.56×10^{-7}	0.028	0.070(10)	e	344	39	14
Projectile Target: $^{14}N/^{58}Ni$									
35	1.8	.34	0.1×10^{-7}	0.061	0.120(15)	e	395	55	14
Projectile Target: $^{14}N/^{184}W$									
35	3.0	.26	0.74×10^{-7}	0.058	0.160(20)	e	440	97	14
Projectile Target: $^{40}Ar/^{40}Ca$									
44	2.1	0.33	4.7×10^{-7}	0.33	2.2(4)	f	880	87	40
Projectile Target: $^{40}Ar/^{119}Sn$									
44	3.14	0.27	3.1×10^{-6}	0.6	3.7(8)	f	1257	147	40
Projectile Target: $^{40}Ar/^{238}$									
44	4.2	0.23	3.1×10^{-6}	2.9	6.(3)	f	1375	202	40

a) calculated as $(1.2(A_T^{1/3} + A_p^{1/3}) \times 10^{-13})^2 \cdot \pi$ where A_T and A_p are target and projectile mass numbers.

b) attenuation factors, calculated as described in the text.

c) this is the product of the calculated reaction cross section times calculated pions per interaction times attenuation factor.

d) H. Noll et al., Phys. Rev. Lett. 48, 732 (1982).

e) J. Stachel et al., in Proceedings of the Institute for Nuclear Studies; RIKEN Symposium on Heavy Ion Physics, Tokyo, Japan, August 1984 (to be published).

f) H. Heckwolf et al., Z. Phys. A315, 243 (1984).

g) Composite nucleus excitation energy.

h) Equilibrium quasiparticle number for composite nucleus excitation.

i) Initial exciton number assumed in calculating pion production cross sections.

$$\sigma_R = \pi \cdot [1.2 \times 10^{-13}(A_T^{1/3} + A_p^{1/3})]^2 \quad . \tag{13}$$

Results of Eq. (6) for the target-projectile combinations considered herein are summarized in Table VI.

7. RESULTS AND DISCUSSION

In Fig. 6 we show experimental π° production cross sections for 35 MeV/nucleon ^{14}N with targets of ^{27}Al, ^{58}Ni and ^{184}W, compared with calculated results as described in Section 6. The calculated results in Fig. 6 result from assuming a Fermi energy of 35 MeV and a distribution function characterized by 14 excitons. These results, and those for the other systems considered, are summarized in Table VI. Generally the calculated results agree to within a factor of two or better with experimental measurements for all cases considered,
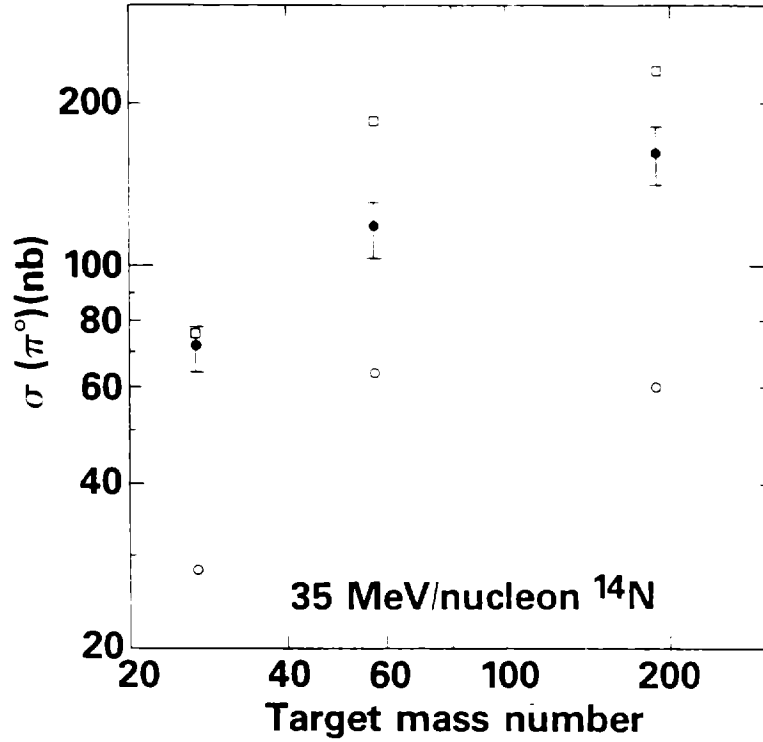
FIG. 6. Experimental and calculated π^0 yields for reactions of 35 MeV nucleon ^{14}N with ^{27}al, ^{58}Ni and ^{184}W targets. The experimental yields are from Ref. (32). The open squares are the calculated yields before multiplication by the attenuation factors noted in the text. The open circles are calculated results after multiplication by the attenuation factors summarized in Table VI.

with the exception of ^{40}Ar + ^{40}Ca at 44 MeV/nucleon incident energy. For this example the calculated yields are low by a factor of 6. We see no obvious explanation for this discrepancy. The direction of discrepancies for the ^{12}C + ^{12}C, ^{58}Ni yields

with increasing projectile energy is consistent with a reaction cross section which decreases with increasing projectile energy, a reasonable expectation not contained in the simple Eq. (13) used. The agreement shown between calculated and experimental results in Table VI suggests that the nucleon–nucleon collision mechanism may very well be one viable explanation of the yields of subthreshold pion production.

If this is the case, then the pion production provides a probe of the very early time history of a heavy ion reaction, as indicated in Fig. 7. The production rate of pions via the two body mechanism may be seen to go rapidly to zero after coalescence is complete, while the nucleon emission rate decreases much more slowly, finally asymptotically approaching an equilibrium emission rate of the order of 10% of the maximum pre–equilibrium rate. Pion production is therefore seen to be extremely sensitive to the primary exciton distribution, and quite insensitive to the distribution after even partial relaxation of the excited Fermi gas.

It has been suggested that subthreshold pion production results from the compound nucleus.[35,36] Such calculations should recognize that a great deal of excitation will be removed by nucleon emission prior to achieving equilibrium. In Table VII we summarize predictions of the BME calculation described in this work, for the average compound nucleus excitation to be expected for several of the 'subthreshold' systems which have been investigated experimentally. The total excitations in several cases are far below the absolute pion production thresholds. All are at considerably lower excitations than the maximum excitation available to the composite systems. Stated differently, only an extremely small fraction of an ensemble of composite systems (for the cases summarized in Table VII) might reasonably be expected to equilibrate prior to precompound decay. Pion
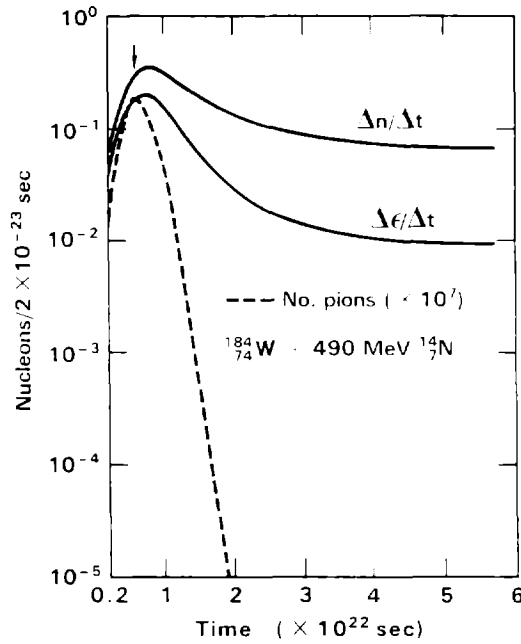
FIG. 7. Calculated π^0, neutron emission, and de-excitation rates versus time from the boltzmann master equation. The down arrow shows the time at which coalescence is considered to be complete in the BME. These results are for ^{184}W + 490 MeV ^{14}N. The rate of energy loss is on a relative scale on the ordinate. The abscissa gives pion or nucleon emission rates per time unit of 2×10^{-23} sec.

production calculations for compound nuclei must find a reasonable method of calculating this fraction if the results are to be relevant to comparisons with experimental yields.

For interest we have summarized the most probable equilibrium quasi-particle numbers at maximum excitation energy for the systems considered herein. These are presented in the next to last column of Table VI. The quasi-particle numbers actually used for the initial energy partitions in the BME are shown in the last column of Table VI. All systems must evolve from an initial condition very far from equilibrium.

TABLE VII. Average excitation energy at equilibrium calculated by Boltzmann equation for several systems.

Target	Projectile	E_{LAB}(MeV)	E_{CN}(MeV)$^{(a)}$	E_{EQ}(MeV)$^{(b)}$
^{184}W	^{14}N	490	440	197
^{58}Ni	^{14}N	490	395	190
^{27}Al	^{14}N	490	344	123
^{12}C	^{12}C	720	374	85
^{12}C	^{12}C	888	458	99
^{12}C	^{12}C	1008	518	100

(a)   Composite nucleus maximum excitation energy
(b)   Calculated average excitation energy of equilibrated nuclei after precompound decay.

Pion spectra from the Boltzmann master equation are compared with experimental results in Fig. 8. The calculated results are seen to be too hard compared with experimental spectra. However the higher energy pions would be more likely to interact through the Δ resonance, and this would tend to soften the spectrum of observed pions. The disagreement in spectral shape is therefore qualitatively in the proper direction.

8.   CONCLUSIONS

The nucleon–nucleon collision mechanism which has been used to explain pion production in nucleon–nucleus collisions is a viable candidate to explain so called 'sub–threshold' pion production. The latter refers to reactions in which a heavy ion projectile has an energy per nucleon below the N–N–π production threshold, but total CM energy in excess of the threshold value.

40
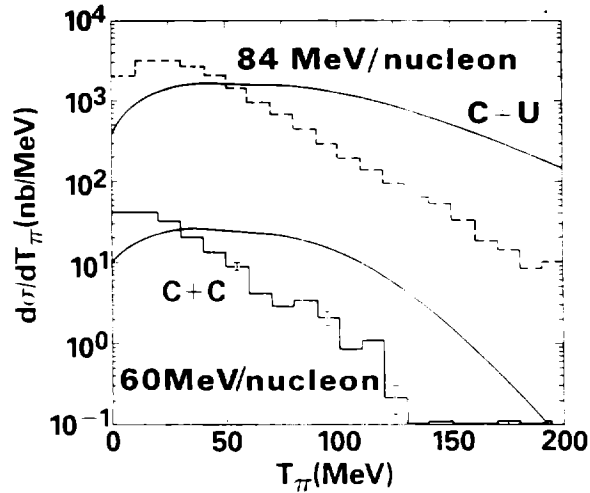
FIG. 8. Calculated and experimental π° spectra for 60 MeV/nucleon ^{12}C + ^{12}C, and for ^{84}MeV/nucleon ^{12}C + ^{238}U. Experimental results are from Ref. (33).

Uncertainties in the input parameters of the calculation relating to the high energy tail of the energy distribution of coalescing nucleons introduce large uncertainties in the quantitative significance of the results of these calculations at this time. Experimental measurements of the nucleon emission spectra for central collisions and for nucleons in excess of ≈ 110 MeV should reduce the ambiguity in input for calculations of this type, thereby increasing confidence in the quantitative results of such calculations.

9. ACKNOWLEDGEMENTS

M. BLANN

REFERENCES

1. G. D. HARP, J. M. MILLER and B. J. BERNE, Phys. Rev. 165, 1166(1968).
2. G. D. HARP and J. M. MILLER, Phys. Rev. C3, 1847(1971).
3. M. BLANN, A. MIGNEREY and W. SCOBEL, Nukleonika 21, 335(1976).
4. M. BLANN, Phys. Rev. 23, 205(1981).
5. M. BLANN, Ann. Rev. Nucl. Sci. 25, 123(1975).
6. M. BLANN, Nucl. Phys. A235, 211(1974).
7. J. RANDRUP, Ann. Phys. (N.Y.) 112, 356(1978).
8. W. J. SWIATECKI, Nucl. Phys. A376, 275(1982).
9. S. COHEN, F. PLASIL and W. J. SWIATECKI, Ann. of Phys. (N.Y.) 82, 557(1974).
10. T. E. O. ERICSON, Adv. Phys. 9, 423(1960).
11. E. L. POLLOCK, private communication (1984).
12. E. HOLUB, et al., Phys. Rev. C28, 252(1983).
13. G. MANTZOURANIS, H. A. WEIDENMULLER and D. AGASSI, Z. Phys. A276, 145(1976).
14. M. BLANN, W. SCOBEL and E. PLECHATY, Phys. Rev. C30, Nov.(1984).
15. W. SCOBEL, et al., Phys. Rev. C30, Nov. (1984); Lawrence Livermore National Laboratory, Livermore, CA, UCID–20101 (1984) unpublished.
16. M. BLANN, R. R. DOERING, A. GALONSKY, D. M. PATTERSON and F. E. Serr, Nucl. Phys. A257, 15(1976).
17. F. E. BERTRAND, R. W. PEELLE and C. KALBACH–CLINE, Phys. Rev. C10, 1028(1974).
18. J. R. WU, C. C. CHANG and H. D. HOLMGREN, Phys. Rev. C19, 698(1979).
19. T. C. AWES, et al., Phys. Rev. C25, 2361(1982).
20. J. BISPLINGHOFF, Workshop on Coincident Particle Emission From Continuum States (Honnef, Germany, 1984) unpublished.
21. Y. D. CHAN, et al, Phys. Rev. C27, 447(1983).
22. B. B. BACK, et al., Phys. Rev. C22, 1927(1980).
23. V. E. VIOLA, et al., Phys. Rev. C26, 178(1982).
24. H. MORGANSTERN, et al., Phys. Lett. 113B, 463(1982).
25. E. DUEK, et al., Z. Phys. A307, 221(1982).
26. W. J. NICHOLSON and I. HALPERN, Phys. Rev. 116, 175(1958).
27. S. S. KAPOOR, H. BABA and S. G. THOMPSON, Phys. Rev. 149, 965(1966).
28. V. E. VIOLA, et al., Nucl. Phys. A261, 174(1976).
29. T. SIKKELAND, E. L. HAINES and V. E. VIOLA, Jr., Phys. Rev. 125, 1350(1962).
30. J. GALIN, et al., Phys. Rev. Lett. 48, 1787(1982).

31. J. JASTREBSKI, private communication (1984).1.

32. P. BRAUN–MUNZINGER et al., Phys. Rev. Lett. 52, 255 (1984).

33. T. JOHANSSON et al., Phys. Rev. Lett. 48, 732 (1982).

34. H. NOLL et al., Phys. Rev. Lett. 52, 1284 (1984).

35. C. GALE and S. DAS GUPTA, Phys. Rev. C 30, 4141 (1984).

36. J. AICHELIN and G. BERTSCH, Phys. Lett. 138B, 350 (1984).

37. J. AICHELIN, Phys. Rev. Lett. 52, 2340 (1984).

38. D. VASK, H. STOECKER, B. MUELLER, and W. GREINER, Phys. Lett. 93B, 243 (1980).

39. R. SHYAM and J. KNOLL, Gesellschaft für Schwerionen-forschung Report No. GSI 83–22, 1983 (unpublished).

40. H. HECKWOLF et al., Z. Phys. A315, 243 (1984).

41. J. STACHEL et al., in Proceedings of the Institute for Nuclear Studies_KIKEN Symposium on Heavy Ion Physics, Tokyo, Japan, August 1984 (to be published).

42. H. KRUSE, B. V. JACEK and H. STOCKER, Phys. Rev. Lett. 54, 289 (1985).

43. M. BLANN, Phys. Rev. Lett. 54, 2215 (1985).

44. G. F. BERTSCH, Phys. Rev. C 15, 713 (1977).

45. B. J. VER WEST and R. A. ARNDT, Phys. Rev. C 25, 1979 (1982).

46. M. BLANN, A. MIGNEREY, and W. SCOBEL, Nukleonika 21, 335 (1976).

47. M. BLANN, Phys. Rev. 23, 205 (1981).

48. P. BRAUN–MUNZINGER, private communication (1984).